

# Theory of phonon dynamics in an ion trap

T. Dutta,<sup>(1)</sup> M. Mukherjee,<sup>(1,2,3)</sup> K. Sengupta<sup>(4)</sup>

<sup>(1)</sup> *Centre for Quantum Technologies, National University Singapore, Singapore 117543, Singapore.*

<sup>(2)</sup> *Physics Department, National University of Singapore, 2 Science Drive 3 Singapore 117551, Singapore.*

<sup>(3)</sup> *Majulab (UMI3654) International Joint Research Unit CNRS-UNS-NUS-NTU, Singapore.*

<sup>(4)</sup> *Theoretical Physics Department, Indian Association for the Cultivation of Science, Jadavpur, Kolkata-700032, India.*

(Dated: January 9, 2018)

We develop a theory to address the non-equilibrium dynamics of phonons in a one-dimensional trapped ion system. We elaborate our earlier results obtained in Phys. Rev. Lett. **111**, 170406 (2013) to chart out the mechanism of dynamics-induced cooling and entanglement generation between phonons in these systems when subjected to a linear ramp protocol inducing site-specific tuning of on-site interactions between the phonons. We further extend these studies to non-linear ramps and periodic drive protocols and identify the optimal ramp protocol for minimal cooling and entanglement generation time. We qualitatively address the effect of noise arising out of fluctuation of the intensity of the laser used to generate entanglement and provide a detailed discussion of a realistic experimental setup which may serve as a test bed for our theory.

PACS numbers:

## I. INTRODUCTION

Trapped ion systems, similar to their cold atom counterparts, are well known emulators of specific models of strongly correlated quantum systems such as the Ising and the Bose Hubbard models [1, 2]. A typical example of such a system constitutes a linear chain of ions in a trap [3, 4]. The physics of the phonons, which are the motional quanta of these charged ions in the trap, can be shown to be described, under appropriate conditions, by the Bose-Hubbard model (BHM) [2]. This leads to the realization of one-dimensional (1D) Bose-Hubbard model in such systems. The equilibrium properties and quantum ground states of these phonons has already been studied theoretically in details [2, 5]. In particular, it was shown that such system may be the perfect test bed for studying the quantum phase transition between the localized Mott and the delocalized superfluid states of the phonons [2, 5, 6].

The key difference between emulation of such correlated model Hamiltonians using trapped ions [7] and ultracold atoms [8–10] are two fold. First, in contrast to their ultracold atom counterparts, trapped ion systems provide easier local control over the parameters of the model. For example, the local interaction potentials between the phonons at a given site can be experimentally tuned for individual sites of the chain. Second, ion trap systems are usually prepared in form of 1D chains; in contrast to their cold atom counterparts, it is not easy to prepare coherent higher dimensional configurations of ions in traps. The second feature makes such system an ideal choice of for studying correlated physics in low-dimension (1D) while the first allows for local control over systems parameters which is very difficult to achieve in cold atoms.

A feature of the trapped ion systems which is of key interest to the present study is that they allow one to study the non-equilibrium dynamics of the model they

emulate. This feature is somewhat similar to ultracold atom emulator; however, the trapped ion system allow us to dynamically change local system parameters with arbitrary precision. Consequently, one can study the non-equilibrium dynamics of the emulated model under local protocols. Since these ion trap systems can be used to emulate correlated models which harbors quantum phase transitions, they provide us with an unique opportunity to study the effect of local non-equilibrium dynamics near a quantum critical point [11, 12]. Moreover, trapped ions are ideal system to test atomic physic at high precision [13] in a controlled and clean way which makes them ideal units for realization of a quantum computer.

In this work, we study the effect of non-equilibrium dynamics of the Bose-Hubbard model, which describes the phonons in a linear chain of trapped ions, under local protocols. The kinetic energy of these phonons is described by a nearest neighbor hopping term while the interaction between them is local (on-site). Such a Hamiltonian can be written as

$$H = J \sum_{\langle ij \rangle} (b_i^\dagger b_j + \text{h.c.}) + \sum_i U_i \hat{n}_i (\hat{n}_i - 1) \quad (1)$$

where  $J > 0$  is the hopping amplitude,  $U_i$  is the on-site interaction between the phonons at the  $i^{\text{th}}$  site,  $b_j$  is the annihilation operator for the phonon at the  $j^{\text{th}}$  site, and  $\hat{n}_i = b_i^\dagger b_i$  is the boson number operator. In what follows we discuss the non-equilibrium dynamics when  $U_i$  is ramped to  $-U_i$  on either one or two of the sites in a chain. We show that the first protocol leads to cooling of the ions to their transverse motional ground state while the second leads to generation of an entangled Bell state between the two sites. We note that our proposal provides an viable alternative for cooling of a long chain of ions which, in contrast to well-known sympathetic cooling [14], does not require the presence of multiple species of ions and provides a cooling time which is independent of the electronic structure of the involved ions. Fur-

ther, our study reveals that non-equilibrium dynamics can be utilized to generate pure many-body entangled states which are computationally relevant.

It is well-known that the generation of entangled quantum states is an essential prerequisite for quantum computation; the present work analyzes a few "experimentally relevant" classes of possible dynamic protocols for generating such a state. In particular, our work here extends the analysis of Ref. 12 to both non-linear and periodic drive protocols. We show that ramp protocols are more efficient compared to periodic ones for cooling and entanglement generation and that the optimal ramp protocol for shortest cooling and entanglement generation time corresponds to a non-linear ramp with exponent  $\alpha \simeq 0.8$ :  $U_i(t) = U_i^{(0)}(1 - 2(t/\tau)^\alpha)$ . Here  $U_i^{(0)}$  is the initial value of the interaction at site  $i$  and  $\tau$  is the ramp time. We also show that the cooling (entanglement generation) can be reliably achieved by single(two) site addressing, *i.e.*, the cooling (entanglement) times do not drastically differ if the on-site interaction on other sites of the chain have a near zero value. Further, we qualitatively address the issue of the effect of the presence of noise, arising out of fluctuation of the intensity of the laser used to generate the on-site interaction, on the entanglement generation and provide an estimate of the maximal effective noise temperature beyond which such entanglement is lost. We note that single(two) site addressing protocols are much easier to achieve experimentally while the noise arising out of laser intensity fluctuations is an inherent part of any ion trap system. Thus a discussion of these issues is expected to make the theory developed here useful to experimentalists working in ion trap systems.

The plan of the rest of the paper is as follows. First, in Sec. II, we provide a detailed discussion of the experimental ion trap system which can act as test bed of our theoretical idea and discuss how such a system can lead to emulation of the Bose-Hubbard model with Hamiltonian given by Eq. 1. This is followed by Sec. III, where we discuss the theoretical method used to study the non-equilibrium dynamics of the model for several local protocols. In Sec. IV, we discuss the results obtained from this study and identify the optimal protocols for cooling and entanglement generation. We provide a qualitative discussion of the effect noise on entanglement generation, summarize our results, and conclude in Sec. V.

## II. ION TRAP SYSTEM

In this section, we discuss the realization of an effective Bose-Hubbard model for the transverse motional modes in a system of trapped ion linear chain starting from their vibrational dynamics. For definiteness, we consider a string of  $N$  positively charged ions with mass  $m$  confined using a linear Paul trap as shown in Fig. 1 [3, 13, 15, 16]. The RF voltage provides a confinement along the radial direction whereas the axial confinement of ions is

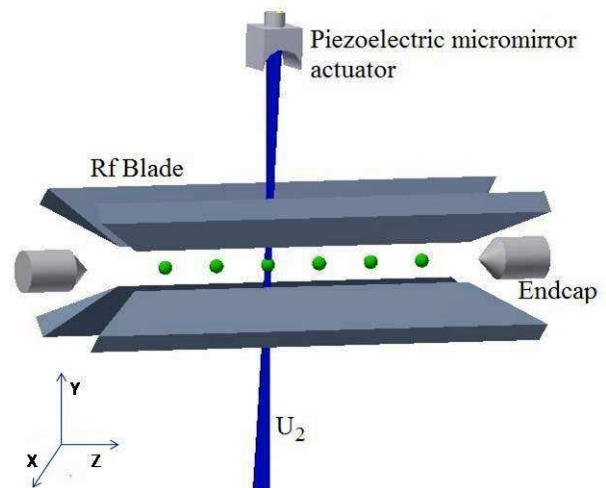


FIG. 1: (Color online) Schematic of the experimental setup. In a linear chain of 6 ions, the third ion (site no. 2) is addressed by an off-resonant laser to generate an on-site interaction  $U_2$ . The axis joining the two endcap electrode is considered as the  $z$ -axis.

achieved by applying dc voltage at the end electrodes. The Hamiltonian describing the vibrational motions in such a trap is given by

$$H_0 = \sum_{i=1}^N \frac{\vec{P}_i^2}{2m} + V_T + V_C. \quad (2)$$

Here  $\vec{P}_i$  is the momenta of the  $i^{\text{th}}$  ion,  $V_C$  is the coulomb potential between any pair of the ions which can be expressed as

$$V_C = \frac{1}{2} \sum_{i,j=1, j \neq i}^N \frac{e^2}{\sqrt{(x_i - x_j)^2 + (y_i - y_j)^2 + (z_i - z_j)^2}}, \quad (3)$$

where  $x_i$ ,  $y_i$ , and  $z_i$  denote the coordinate of the  $i^{\text{th}}$  ion in three orthogonal directions, and  $V_T$  is the trapping potential, which determines the equilibrium positions of the ions and is given by

$$V_T = \frac{m}{2} \sum_{i=1}^N (\omega_x^2 x_i^2 + \omega_y^2 y_i^2 + \omega_z^2 z_i^2). \quad (4)$$

Here  $\omega_x, \omega_y, \omega_z$  are the radial and longitudinal trap frequencies. In what follows, we are going to work in the regime  $\omega_x, \omega_y \gg \omega_z$  so that the ions are strongly confined in the radial direction. In our setup, the chain direction is taken to be along  $z$  as shown in the Fig. 1. The oscillations of ion along the radial directions, in this regime, is small compared to the inter-ion distance.

Both the trapping potential and Coulomb repulsion determines the equilibrium position of ions. In the regime

described above, the Coulomb potential is much weaker compared to the radial confinement, and the displacements of ions in any direction can be considered to be decoupled from the other two orthogonal directions allowing us to discuss the vibrational modes in the radial direction only. To this end, we expand  $V_C$  as a function of radial displacement around the equilibrium ion position and obtain the Hamiltonian

$$H_x = \sum_{i=1}^N \left[ \frac{P_{i,x}^2}{2m} + \frac{m}{2} \omega_x^2 \delta x_i^2 \right] + \frac{1}{2} \sum_{\substack{i,j=1 \\ (i>j)}}^N \frac{e^2 (\delta x_i - \delta x_j)^2}{|d_{ij}^0|^3}, \quad (5)$$

where  $|d_{ij}^0| = |z_i^0 - z_j^0| = d_0 |i_z - j_z|$  is the mean distance between  $i^{\text{th}}$  and  $j^{\text{th}}$  ion along the  $z$ -direction,  $i_z(j_z)$  are the site number of the  $i^{\text{th}}(j^{\text{th}})$  site,  $d_0$  is the inter-site distance between neighboring ions, and  $\delta x_i$  is the radial displacements of the  $i^{\text{th}}$  ion around its radial equilibrium positions. The second quantized form of this Hamiltonian can be obtained following standard methods [17] and takes the following form ( $\hbar = 1$ ):

$$H_x = \sum_{\substack{i,j=1 \\ i>j}}^N J_{ij} (b_i^\dagger b_j + h.c.) + \sum_{i=1}^N (\omega_x + \omega_{x,i}) b_i^\dagger b_i \quad (6)$$

Here  $b_i$  denotes the annihilation operator for phonons (quanta of vibrational displacement modes) in the radial direction, and the hopping amplitude  $J_{ij}$  is induced by the Coulomb interaction. The effective trapping frequency,  $\omega_{x,i}$  depends on the ion's positions, as well as the tunneling amplitudes  $J_{ij}$  and is given by

$$\omega_{x,i} = \omega_x - \sum_{\substack{j=1 \\ (j \neq i)}}^N \frac{e^2}{2m\omega_x |d_{ij}^0|^3}, \quad J_{ij} = \frac{e^2}{2m\omega_x |d_{ij}^0|^3}. \quad (7)$$

In this context, it is customary to define the dimensionless parameter  $\beta_x$  as the ratio of the Coulomb energy between near-neighbor sites to the trapping potential energy:

$$\beta_x = e^2 / (m\omega_x^2 d_0^3). \quad (8)$$

The parameter  $\beta_x$  characterizes the normal modes of the system in radial direction; when  $\beta_x \gg 1$ , the Coulomb repulsion dominates over the trapping potential. In this case, the long-range nature of the Coulomb interaction becomes important and the effect of the collective motion along the axial direction is expected to play important role in the collective motion of the ions and can not be ignored. However, in the limit  $\beta_x \ll 1$ , the Coulomb interaction is effective between nearest ions only. In this regime, which we focus on, the number non-conserving term in the effective Bose-Hubbard Hamiltonian such as  $(b_i b_j, b_i^\dagger b_j^\dagger)$  can be neglected since they lead to an energy cost which is larger than the Coulomb energy. We

have used this fact to arrive at Eq. 6. Also, since the Coulomb interaction is effective only between the nearest neighboring sites, one can express  $J_{i,j}$  in terms of  $\beta_x$  as

$$J_{ij} \approx J \delta_{i,j \pm 1}, \quad J = \beta_x \omega_x / 2. \quad (9)$$

Note that for  $\beta_x \ll 1$ , the effect of on-site phonon-phonon interaction is negligible due to the small amplitude of anharmonicity in the trap which arises from the imperfection of trap architecture. However, in a realistic system, this effect can be enhanced and controlled by introducing off resonant standing wave along the transverse direction of the trap axis. The bosonic Hamiltonian, in the presence of such a standing wave, has an additional term

$$H_I = F \sum \cos^2(kx_i + \frac{\pi}{2}\delta), \quad (10)$$

where  $F$  is the peak AC stark shift and  $k$  is the wavevector of the wave. This controllable anharmonicity brings the phonons closer by making unequal the otherwise equally spaced energy levels of radial trap potential. To quantify this effect, one may define the dimensionless Lamb-Dicke parameter  $\eta_x = k \sqrt{\hbar/2m\omega_x} \ll 1$ ; in terms of  $\eta$ , it is possible to write  $H_I$  as

$$H_I = F \sum_{i=1}^N [1 + \eta_x^2 (b_i^\dagger + b_i)^2 + \frac{1}{3} \eta_x^4 (b_i^\dagger + b_i)^4 + \theta(\eta_x)^6]. \quad (11)$$

In the regime where  $F\eta^2 \ll \omega_x$ , the effective interaction between the bosons is quartic and can be written as

$$H_I = (-1)^\delta F \eta_x^4 / 3 \sum_{i=1}^N (b_i + b_i^\dagger)^2 \simeq \sum_i U_i b_i^{\dagger 2} b_i^2, \quad (12)$$

where in arriving at the last relation we have used the fact that the number non-conserving terms such as  $b_i^2, b_i^{\dagger 2}$  can be neglected since they corresponds to much higher energy scales as discussed earlier. Also, it can be shown that the rest of the phonon conserving terms will induce a small shift in the radial potential which amounts to a re-definition of the the overall potential. The above discussion leads to the final form of the Bose-Hubbard Hamiltonian given by Eq. 1 with  $J > 0$  and  $U_i = 2(-1)^\delta F \eta_x^4$ . The on-site interaction strongly depends on the strength of the standing wave and relative position ( $\delta = 0$  or  $1$ ) of ion on the standing wave. Note that it is possible to have  $U_i$  to be repulsive or attractive which is one of the key facts used in the present work. Finally, it is useful to note that the sign of the hopping term in the present Bose-Hubbard model is positive in contrast to its ultra-cold atom counterpart where such a term comes with a negative sign.

### III. METHOD FOR STUDYING NON-EQUILIBRIUM DYNAMICS

In this section, we outline our method for studying non-equilibrium dynamics of the 1D Bose-Hubbard

model (Eq. 1) derived earlier. We begin by specifying the protocols for the dynamics that we study. We start with the system in the ground state of the Hamiltonian given by Eq. 1 for a fixed  $J$  and  $U_i$ . We consider a chain of  $N$  ions; the choice of  $N$  depends on experimental setting which is to be discussed in Sec. V.

The dynamics is induced in the model by changing the local interaction parameter  $U_i^{(0)}$  to  $U_i^{(1)} = -U_i^{(0)}$  on a one or more selected site(s). For cooling, we change  $U_i$  at any one of the  $N$  sites, while for generating entanglement this change is made for local interactions on two of the sites of the chain. The protocol used to make such a change are either linear or non-linear ramp or periodic and are given by

$$\begin{aligned} U_i(t) &= U_i^{(0)}[1 - 2(t/\tau)^\alpha], \quad 0 \leq t \leq \tau, \quad (\text{ramp}) \\ &= U_i^{(0)} \cos(\pi t/\tau), \quad 0 \leq t \leq \tau, \quad (\text{periodic}) \end{aligned} \quad (13)$$

where the exponent  $\alpha$  specifies the power-law which is followed by the ramp and  $\alpha = 1$  indicates linear ramp protocol studied in Ref. 12. We note here that  $\tau \rightarrow 0$  indicates the sudden quench limit; such dynamics for the model was studied in Ref. 11. In case of periodic ramp, we would be using  $T$  and  $\omega_0$  to denote the period and frequency of the ramp which is related to  $\tau$  as  $\tau = T/2 = \pi/\omega_0$ .

To study the dynamics, we begin at  $t = 0$  assuming that the system is in the ground state of the Bose-Hubbard model given by Eq. 1 with  $U_i^{(0)} = U^{(0)} > 0$  at all sites and a fixed  $J/U^{(0)}$  at each site. Since we work in a regime where changing the number of phonons is a high-energy process, we shall study the dynamics at fixed number  $N_0$  total phonons (bosons). Thus the Hilbert space of the bosons can be truncated to keep those states for which  $n_i \leq N_0$  for any site  $i$ . We use exact diagonalization method for the finite-size system within this truncated Hilbert space to obtain the energy eigenstates  $|\alpha\rangle$  and eigenvalues  $E_\alpha$  for  $H(t = \tau)$ . This amounts to a choice of basis; in terms of these eigenstates, one can express the initial ground state (at  $t = 0$ )

$$|\psi_G\rangle = \sum_{\alpha} c_{\alpha}^0 |\alpha\rangle, \quad (14)$$

where the coefficients  $c_{\alpha}^0$  denote the overlap of the initial ground state of the system, also obtained using exact diagonalization in the same truncated Hilbert space with  $H = H(t = 0)$ , with  $|\alpha\rangle$ .

The time-dependent Schrödinger equation for the system wavefunction

$$|\psi(t)\rangle = \sum_{\alpha} c_{\alpha}(t) |\alpha\rangle \quad (15)$$

governing the dynamics of the system now reduces to equations for time evolution of  $c_{\alpha}(t)$ :

$$i\hbar\partial_t \sum_{\alpha} c_{\alpha}(t) |\alpha\rangle = H(t) \sum_{\alpha} c_{\alpha}(t) |\alpha\rangle \quad (16)$$

with the boundary condition  $c_{\alpha}(0) = c_{\alpha}^0$ . To solve these equations, it is convenient to rewrite

$$\begin{aligned} H(t) &= H(\tau) + \Delta H(t), \\ \Delta H(t) &= \sum_i (U_i(t) - U_i(\tau)) \hat{n}_i (\hat{n}_i - 1). \end{aligned} \quad (17)$$

With this choice, one obtains the final set of equations for  $c_{\alpha}(t)$  to be

$$\begin{aligned} (i\hbar\partial_t - E_{\alpha})c_{\alpha}(t) &= \sum_{\beta} \Lambda_{\alpha\beta}(t)c_{\beta}(t) \\ \Lambda_{\alpha\beta}(t) &= \langle\beta|\Delta H(t)|\alpha\rangle. \end{aligned} \quad (18)$$

The set of coupled equations for  $c_{\alpha}(t)$  is then solved numerically leading to an exact numerical solution for the time-dependent boson wavefunction  $|\psi(t)\rangle$ . We note here that it is clear from the structure of Eq. 18 that  $c_{\alpha}(t)$  can be written as

$$\begin{aligned} c_{\alpha}(t) &= \tilde{c}_{\alpha}(t)e^{-iE_{\alpha}t/\hbar} \\ i\hbar\partial_t \tilde{c}_{\alpha}(t) &= \sum_{\beta} e^{i(E_{\beta} - E_{\alpha})t/\hbar} \Lambda_{\alpha\beta}(t) \tilde{c}_{\beta}(t) \end{aligned} \quad (19)$$

Having obtained the wavefunction  $|\psi(t)\rangle$ , one can compute the expectation value and equal-time correlation functions corresponding to any boson operator as a function of time. This is given, for a local boson operator  $\hat{O}_j$ , as

$$\begin{aligned} O_j(t) &= \langle\psi(t)|\hat{O}_j|\psi(t)\rangle \\ &= \sum_{\alpha\beta} \tilde{c}_{\beta}^*(t)\tilde{c}_{\alpha}(t)e^{i(E_{\beta} - E_{\alpha})t/\hbar} \langle\beta|\hat{O}_j|\alpha\rangle \\ C_{jk}^{nm;O}(t) &= \langle\psi(t)|\hat{O}_j^n \hat{O}_k^m |\psi(t)\rangle \\ &= \sum_{\alpha\beta} \tilde{c}_{\beta}^*(t)\tilde{c}_{\alpha}(t)e^{i(E_{\beta} - E_{\alpha})t/\hbar} \langle\beta|\hat{O}_j^n \hat{O}_k^m |\alpha\rangle, \end{aligned} \quad (20)$$

where  $n, m$  are arbitrary integers and  $j, k$  denote site indices. Although our method is powerful enough to allow us to compute the expectation and correlation corresponding to any bosonic operator  $\hat{O}$ , in what follows, we shall be mainly interested in obtaining these quantities pertaining the boson annihilation operators  $b_j$  and the number operators  $\hat{n}_j = b_j^\dagger b_j$ .

Before ending this section, we briefly comment about the single/two-site addressing protocol which we shall use in Sec. IV. For such protocol  $U_i^{(0)} = U^{(0)}$  at  $t = 0$  only on the site(s) where they are dynamically changed during the protocol. For the rest of the sites  $U_i = 0$  at all times. This protocol has the advantage of experimental simplicity, and as we shall, see leads to faster cooling and entanglement generation. We note here that the formalism developed here can be applied for this protocol without any major modification.

## IV. RESULTS

In this section, we present a detailed account of the results obtained by numerical solution of Eqs. 19 followed by evaluation of appropriate expectation value or correlation function by computing Eq. 20. In Sec. IV A, we discuss these results in the context of cooling. This is followed by Sec. IV B where we discuss entanglement generation.

### A. Cooling of ions

To achieve cooling of the ions, we follow the protocol developed in Ref. 12 and change the on-site interaction on one of the lattice sites in the chain from  $U_i^{(0)} \equiv U^{(0)}$  to  $U_i^{(1)} \equiv -U^{(0)}$  with a fixed ramp rate  $\tau^{-1}$ . In Ref. 12, we have studied the linear ramp protocol. Here we concentrate on non-linear ramp protocol characterized by an exponent  $\alpha$  (Eq. 13) with the aim to optimizing the cooling time. For the sake of definiteness, we shall choose a chain of  $L = 8$  site and choose to ramp the interaction on the second site of the chain ( $i = 2$ ). We note that this choice is made for the sake of definiteness and do not lead to loss of generality. In what follows, we study the time evolution of the phonon population on the second site:  $N_2/N = \langle b_2^\dagger b_2 \rangle / N$ . In the rest of this section, we shall set the total phonon number  $N = 4$ .

The results of such a study are shown in Fig. 2.. Fig. 5. In Fig. 2, we plot the phonon number  $N_2$  at the end of the ramp ( $t = \tau$ ) as a function of the ramp time  $\tau$  for

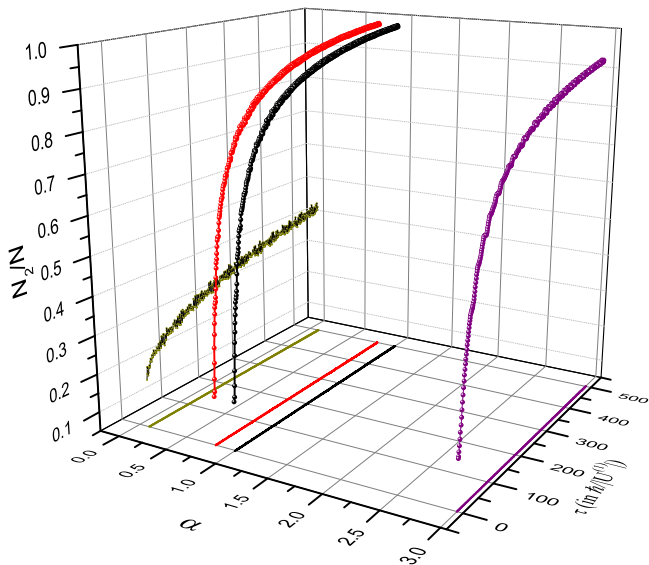


FIG. 2: (Color online) Expectation values of  $N_2/N$  as a function of the ramp time  $\tau$  and exponent  $\alpha$ . Linear ramp is represented by  $\alpha = 1$  while the other three are for exponents 0.1, 0.8 and 3 respectively. For all plots the initial  $J/U_i^{(0)} = 0.2$ . The maximal phonon transfer occurs when  $\alpha = 0.8$ (red).

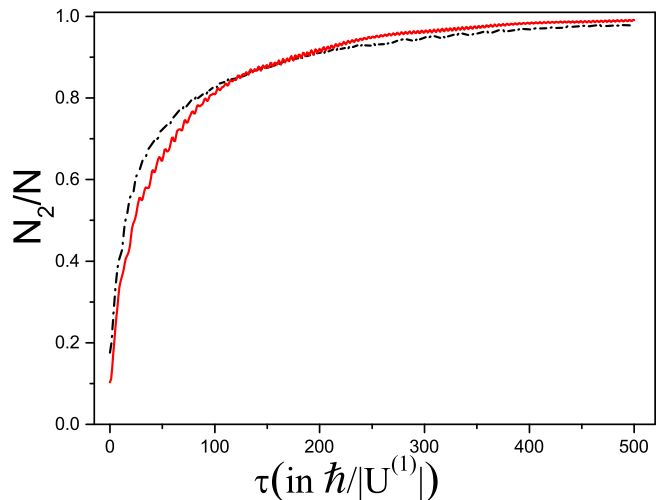


FIG. 3: (Color online) Comparative plot of cooling in case of all site except site no. 2 applied with a repulsive on-site interaction ( $U_i > 0$ ) and no on-site interaction ( $U_i = 0$ ). The dashed-dot curve (black) is same as in Fig. 2 for the optimal exponent  $\alpha = 0.8$  while the solid-line curve is for no on-site interaction except at site number 2. The cooling time remains similar while the final state is cooler in case of no interaction as compared to interaction applied to all sites.

several  $\alpha$  and  $J/U^{(0)} = 0.2$ . We find that, in accordance with our expectation,  $N_2$  approaches  $N$  for slower ramps indicating the migration of the phonons to the second site of the chain leading to cooling of the other sites. By studying the evolution of the phonon number on the second site, we find that  $N_2$  approaches  $N$  in the shortest possible time for  $\alpha \simeq 0.8$ . Thus our study reveals that a non-linear ramp with  $\alpha = 0.8$  is the optimal protocol for cooling. We find that with  $|U^{(1)}| = 2.8\text{kHz}$  on all sites, the linear ramp achieves  $N_2/N = 0.9(0.97)$  for  $t = 12(26)\text{ms}$ ; in contrast a ramp with  $\alpha = 0.8$  with same  $|U^{(1)}|$  leads to  $N_2/N = 0.9(0.97)$  for  $t = 11(24)\text{ms}$ .

Next, to study other aspects of the cooling dynamics, we resort to single site addressing, *i.e.*, we keep the initial interaction parameter  $U_i^{(0)} = U^{(0)}\delta_{i2}$  finite only at the site where it is to be dynamically changed to  $-U^{(0)}$ ; interaction is set to zero for phonons on rest of the sites. The motivation behind such single site addressing is that it is experimentally a lot simpler; further as shown in Fig. 3, such single site addressing does not lead to appreciable change in the nature of  $N_2/N$  as a function of  $\tau$ . In fact, the cooling time corresponding to  $N_2/N = 0.97$  can be further reduced by such single site addressing: for  $\alpha = 0.8$  and  $|U^{(1)}| = 2.8\text{kHz}$ , one reaches  $N_2/N = 0.9(0.97)$  in  $t = 10(19)\text{ms}$ . In the rest of this section, we shall thus concentrate on single site addressing.

We further look for optimization of the parameter  $J/U^{(0)}$  within single site addressing. To this end, we study the behavior of  $N_2/N$  at the end of the ramp ( $t = \tau$ ) as a function of  $J/U^{(0)}$  for several representa-

tive values of  $\tau$  and for  $\alpha = 0.8$ . Our study reveals that the maximal value of  $N_2/N$  occurs at  $J/U^{(0)} \simeq 0.2$ . This leads us to identify  $\tau \geq 500$ ,  $\alpha \simeq 0.8$ , and  $J/U^{(0)} \simeq 0.2$  as optimal ramp parameters for achieving cooling.

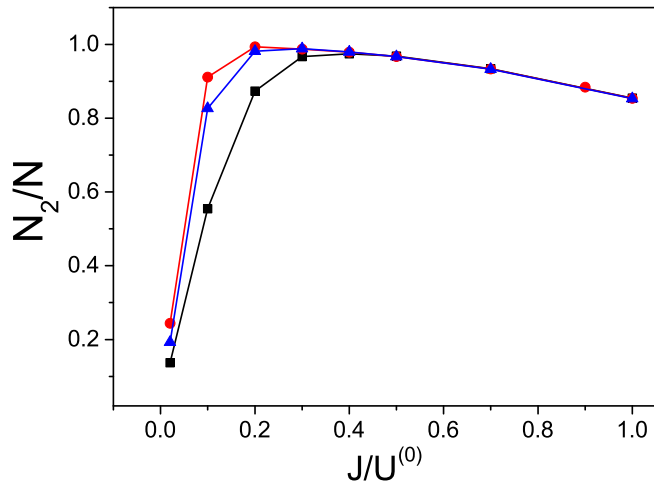


FIG. 4: (Color online) Fractional photon transfer  $N_2/N$  as a function of initial BH parameter  $J/U^{(0)}$  for three different ramp time  $\tau = 100$  (square, black), 300 (triangle, blue), 500 (circle, red) (in units of  $1/|U^{(1)}|$ ). The ramps are non-linear with optimized value of  $\alpha = 0.8$ . In all these cases, the on-site interaction has been applied to a single site 2.

Finally, we compare ramp protocols to periodic protocols, described by Eq. 13, for identifying the optimal protocol for cooling. In what follows, we study the evolution of  $N_2/N$  under such a protocol for  $J/U^{(0)} = 0.2$  and with single site addressing. The result of such a study is shown in Fig. 5. In the top left panel of Fig. 5, we plot  $N_2/N$  at the end of the drive as a function of the drive frequency  $\omega_0$ . We find that  $N_2/N$  has an oscillatory behavior as a function of  $\omega_0$  for small changes in  $\omega_0$ ; however, for a larger variation of  $\omega_0$ , it decreases with increasing  $\omega_0$ . The rest of the panels of Fig. 5 shows the time evolution of  $N_2/N$  for a wide range of  $\omega_0$ . From these plots, we find that one needs a much longer cooling time if periodic protocols are used; for example,  $N_2/N = 0.9(0.97)$  for  $t = 81(88)$ ms with  $\omega_0 = 0.0012$  in terms of  $|U^{(1)}|$ ,  $|U^{(1)}| = 2.8$ kHz and single site addressing. Thus we conclude that ramp protocols perform better than their periodic counterparts for the purpose of cooling. The origin is this behavior can be qualitatively understood as follows. For efficient cooling, one needs to maximize the overlap of the final system wavefunction with the ground state wavefunction. Such an overlap depends on the slope of  $U_i(t)$  at each instant of time. This can be understood by noting that a near zero slope of  $U_i(t)$  is expected to reproduce the adiabatic evolution which will lead to maximal overlap. The slope of  $U_i(t)$  can be optimized more efficiently for ramp protocols by varying the exponent  $\alpha$ . For periodic protocol such as the one described by Eq. 13, the short time ( $\omega_0 t \ll 1$ ) evolution always occur

with a near-zero slope, followed by a steeper increase at intermediate and later times which leads to worse overlap compared to a ramp with optimal exponent. We also note that the ramp protocol advocated here is not necessarily the absolute optimal protocol for the problem [18]; however, it is certainly the most efficient among the experimentally accessible protocols discussed here.

## B. Entanglement generation

In this subsection, we discuss dynamical entanglement generation using the ramp protocol. In doing so, we choose to change the sign of the interaction following the ramp protocol given in Eq. 13 on two symmetrically placed sites on the chain. For definiteness, and without loss of generality, in the rest of this section, we shall choose a chain of length  $L = 6$  with site index  $0 \leq i \leq 5$  and change the on-site interaction for  $k = 1$  and  $l = 4$ . We measure the cross correlation between the these two sites which is given by

$$C_{kl}(t) = \langle \psi(t) | (b_k^\dagger b_l)^N | \psi(t) \rangle / N! \quad (21)$$

We note that if we carried out the protocol of changing the sign of interaction for sites  $k$  and  $l$  adiabatically (with infinitely slow rate;  $\tau \rightarrow \infty$ ),  $C_{14}(t_f = \infty) = C_{14}^{\max} = 1/2$ . Such a correlation, in the present context, pertains to the Bell state between the sites  $k$  and  $l$  given by

$$|\psi_{\text{Bell}}\rangle = \frac{1}{\sqrt{2}} (|0N0000\rangle + |0000N0\rangle), \quad (22)$$

since it yields  $C_{14} = C_{14}^{\max}$ . Thus in the adiabatic limit,  $|\psi\rangle$  generated by the protocol described above is expected

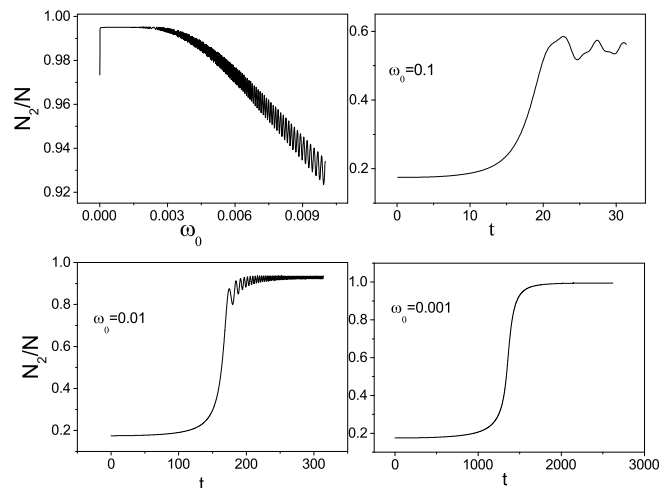


FIG. 5: (Color online) Plot of  $N_2/N$  for periodic ramps: Initial  $J/U^{(0)} = 0.2$  and single site addressing done for all plots. Top-left panel is  $N_2/N$  vs  $\omega_0$  and rest of the figures show  $N_2/N$  as a function of  $t$  for three different values of  $\omega_0$ : 0.1, 0.01, and 0.001 respectively.

to have perfect overlap with the Bell state. However, if the ramp is done fast, as shown in Ref. 12,  $C_{14}(t_f)$  does not reach  $C_{14}^{\max}$  even when  $t_f \gg \tau$ . Since one of the motivations behind generation of entangled state is performing quantum gate operations in the shortest possible time, it is therefore useful to find optimal ramp time  $\tau$  and power  $\alpha$  for which  $C_{14}(t_f)$  reaches a significant fraction of  $C_{14}^{\max}$ . This issue has been investigated for linear ramp protocols in Ref. 12; here we generalize such study to non-linear ramp protocols.

In attempting such generalization, we find that in analogy to the dynamic protocol for cooling of ions, the entanglement generation protocol also yields the shortest time for  $\alpha = 0.8$ . So in what follows, we concentrate on a non-linear ramp with  $\alpha = 0.8$ . Furthermore, in analogy to the cooling protocol, we resort to two-site addressing, *i.e.*, we keep a finite initial interaction only the on two sites where we change the interaction parameter; for the rest of the sites,  $U_i = 0$  at all times. We note that, as shown in Fig. 6, the two-site addressing do not change the dynamics of  $C_{14}(t)$  in any appreciable manner; in fact, such a protocol leads to faster plateauing of  $C_{14}(t)$  which signifies a faster entanglement generation. Thus we shall restrict ourselves to the two-site addressing protocol for the rest of this section.

Next, we study the maximum attained value of the correlation,  $C_{14}^{\max}$ , in a given ramp with exponent  $\alpha = 0.8$  as a function of the ramp time  $\tau$  and  $J/U^{(0)}$ . The corresponding plot, shown in Fig. 7, indicates that it is indeed possible to reach very close to the maximal value 1/2 of

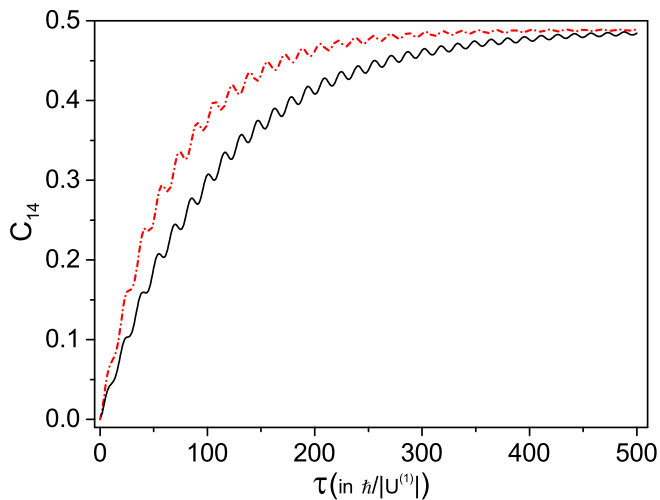


FIG. 6: (Color online) Phonon-phonon correlation between sites 1 and 4  $C_{14}$  as a function of the ramp time  $\tau$  in units of  $U^{(0)}$  for a non-linear ramp of exponent  $\alpha = 0.8$ . The dashed (red) curve is for  $J/U^{(0)} = 0.15$  applied to sites 1 and 4 only, while at the other sites  $U_i = 0$ . The solid-line (black) curve is for all sites initially at  $J/U^{(0)} = 0.15$  while ramp is applied to only sites 1 and 4 while others are kept at  $J/U = 0.15$ . As in case of cooling (see Fig. 3), application of on-site interaction to all sites during the ramp does not make any significant difference.

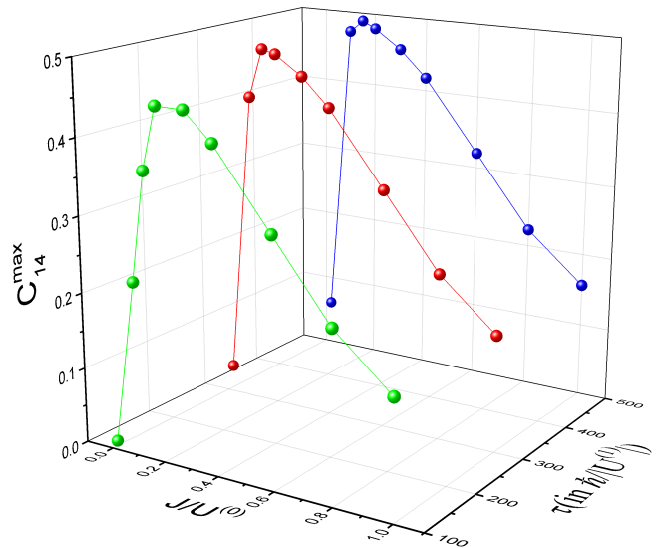


FIG. 7: (Color online) Entanglement generation in terms of cross-correlation as a function of ramp time and initial  $J/U^{(0)}$  value for non-linear ramp of exponent  $\alpha = 0.8$  and two site addressing only.

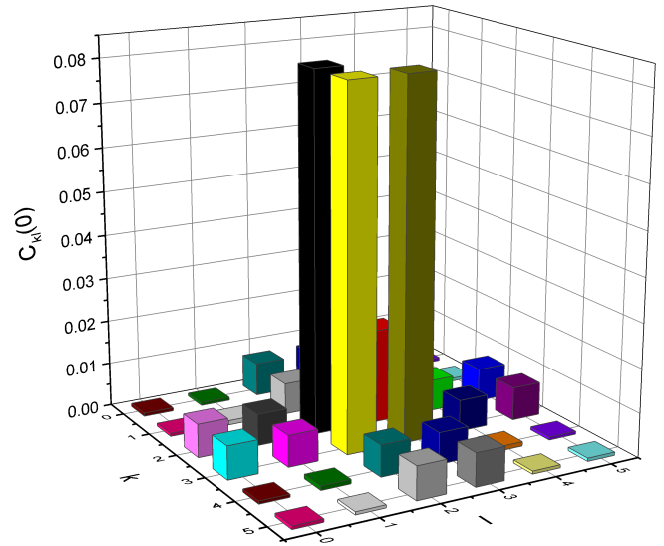


FIG. 8: (Color online) The real part of the density matrix for six site linear chain. In this case the correlation  $C_{kl}(0)$  is for  $J/U^{(0)} = 0.15$  applied to only sites 1 and 4 which has been considered as the initial state.

$C_{14}$  within a finite time; the optimal parameters for this turns out to be  $\tau = 500\hbar/|U^{(1)}|$  and  $J/U^{(0)} = 0.15$ . To show that such a correlation indeed represent realization of a Bell state, we compute the cross correlation between all pairs of sites,  $C_{kl}$  for  $\tau = 500\hbar/|U^{(1)}|$ ,  $\alpha = 0.8$  and  $J/U^{(0)} = 0.15$  for sites  $i = 1$  and  $i = 4$ . At  $t = 0$ , before the ramp is carried out, we find from Fig. 8, that  $C_{kl}(0)$  is finite and has comparable magnitude for most pair of sites. This situation is to be contrasted with the behav-

ior of  $C_{kl}(t = \tau)$ ; as shown in Fig. 9,  $C_{kl}(t = \tau)$  is close of to  $1/2$  for  $k = 1, 4$  and  $l = 1, 4$  and is close to zero otherwise. This is clearly a signature of generation of Bell state through dynamics. We note that this method may also be used to generate entangled states involving multiple sites such as the Greenberger–Horne–Zeilinger state [12]; however generation and maintaining stability of these states are expected to be much more complicated experimentally.

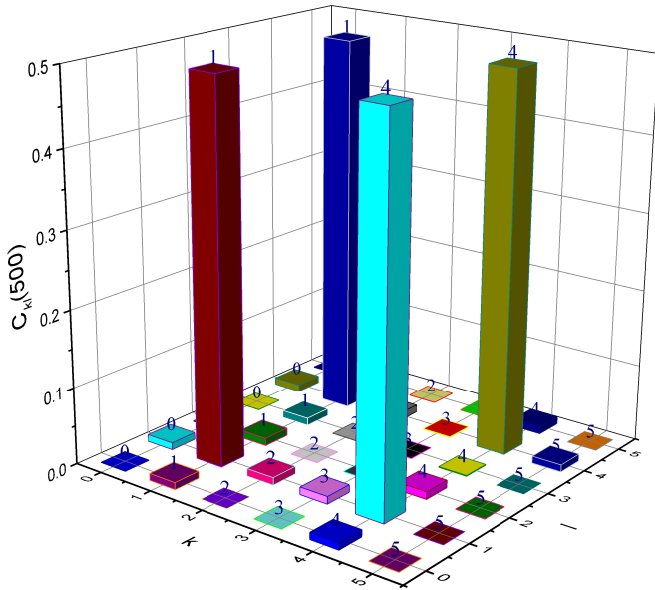


FIG. 9: (Color online) Tomograph for  $J/|U^{(1)}| = 0.15$  with  $U^{(1)} < 0$  for  $k = 1$  and  $4$  and  $U^{(1)} > 0$  otherwise. The other parameters are  $\tau|U^{(1)}|/\hbar = 500$  and  $\alpha = 0.8$ .

Before ending this section, we would like to make a comment regarding the requirement that the sites between which such cross correlation is generated need to be symmetrically placed for a finite chain. This requirement stems from the fact that the on-site energies of these two sites need to be identical for generating a Bell-like state. These on-site energies have contribution from virtual boson hopping processes which are  $O(J^2/U^2)$  or higher. Since the boson hopping processes are cut off by chain ends, these contributions vary with the position of a site; thus two sites which are asymmetrically placed with respect to the chain ends would have different on-site energies due to different contributions from virtual boson hopping processes. Since for creating entangled states involving bosons in two different sites, one needs to have equal on-site energies of the two sites to a high-degree of accuracy, these sites need to be placed symmetrically with respect to the chain ends. Indeed, as shown in Fig. 10, a variation of on-site energy induced by changing the ratio  $U_1^{(1)}/U_4^{(1)}$  from one, leads to a decay of the entanglement. This inherent fragile structure of the entangled state motivates us to at least qualitatively discuss the effect of the presence of noise (which is an integral part of any experiment carried in ion trap sys-

tems) on entanglement generation. We shall discuss this in the next section.

## V. DISCUSSION

In this work, we consider cooling and entanglement generation for an ion trap system with a chain of  $L$  sites with  $N$  phonons. The numbers  $L$  and  $N$  can be controlled and they vary within the range  $2 \leq L \leq 14$  and  $0 \leq N \leq 10$  in typical experimental setups. For cooling, we choose any one ( $i^{\text{th}}$ ) the  $L$  sites with  $U_i^{(0)} = U^{(0)}$  at  $t = 0$  and vary  $U_i(t)$  according to a ramp protocol so that  $U_i^{(1)} = -U^{(0)}$  at the end of the ramp. This leads to migration of phonons to the  $i^{\text{th}}$  sites leading to cooling of the rest of the sites in the system. We find that  $N_i/N \sim 0.97$  for  $\tau \simeq 19\text{ms}$  for a typical  $|U^{(1)}| = 2.8\text{kHz}$  and  $J/U^{(0)} \simeq 0.15$ . Such a cooling time pertains to a chain of  $L = 8$ ; one expects the cooling time to increase linearly with the chain length since the migration time of the phonons  $\sim L\hbar/J$  increases linearly with this length for a fixed  $J$ .

Next, we come to the issue of entanglement generation. As we noted in Sec. IV B, the dynamical generation of entanglement crucially depends on the equality of the on-site energies of the two chosen sites  $i$  and  $j$  of the chain;  $C_{ij}$  falls down rapidly from its maximal value of  $0.97C_{ij}^{\text{max}}$  when these on-site interactions differ from each other. Thus the entangled state generated during dynamics is expected to be fragile against any relative fluctuation of the on-site interactions  $U_i$  and  $U_j$ . Such fluctuations are integral part of a realistic experimental setup since they originate from the fluctuation of the intensity and/or frequency of the lasers used to generate the on-site interactions. Thus any realistic protocol for dynamic generation of entangled state needs to address the effect of noise on  $C_{ij}$ ; in what follows, we qualitatively

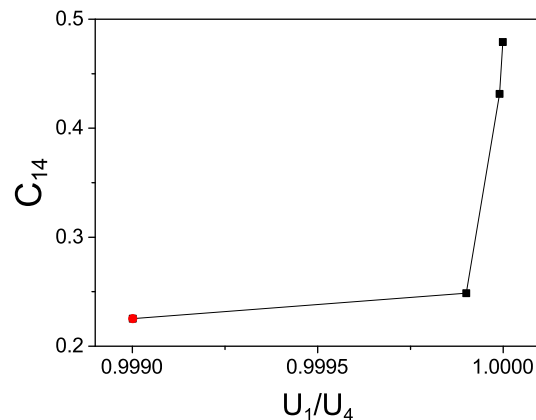


FIG. 10: (Color online) Plot of  $C_{14}(t_f)$  with the ratio of two on-site interaction strengths  $U_1$  and  $U_4$  reflecting the sensitive dependence of the entanglement on the on-site energy.



address this issue.

Assuming that slow drifts can be controlled by suitable locking, the time scale of the laser fluctuations  $\sim 100$ ns are much shorter than typical entanglement generation time  $\tau \sim 20$ ms. Thus in any typical measurement, one expects the effect of noise to self-average; an estimate of  $C_{ij}$  can thus be obtained from its average value over several noise realization. A direct estimate of  $C_{ij}$  thus requires solution of stochastic differential equations given by Eq. 18 with  $U_i(t) \rightarrow U_i(t) + \delta U_i(t)$ , where  $\delta U_i(t)$  denotes the random fluctuation of the on-site interaction on the  $i^{\text{th}}$  site. We do not attempt to solve this problem here. Instead, to obtain a qualitative understanding of the effect of noise, we consider a two site problem with two phonons ( $L = 2$ ,  $N = 2$ ) which are described by the Hamiltonian

$$H_1(t) = J(b_1^\dagger b_2 + \text{h.c.}) + U(t)[\hat{n}_1(\hat{n}_1 - 1) + (1 + \delta U/U(t))\hat{n}_2(\hat{n}_2 - 1)]. \quad (23)$$

Here  $b_1(b_2)$  are the phonon annihilation operators on sites 1(2),  $\hat{n}_i = b_i^\dagger b_i$  is the phonon number operator,  $J$  is the hopping amplitude between the sites,  $U(t) = U^{(0)}(1 - 2(t/\tau)^\alpha)$  is the on-site interaction which is varied from  $U^{(0)}$  to  $-U^{(0)}$  within a ramp time  $\tau$ , and  $\delta U$  is a random number representing the relative fluctuation between the on-site interactions at site 1 and 2. In what follows we shall choose  $\delta U$  to have a Gaussian distribution  $\exp[-x^2/\eta_0^2]$ , where the variance  $\eta_0 = k_B T_{\text{eff}}$  denotes the effective noise temperature of the system.

The Hilbert space of the above model can be charted out in terms of the number states of bosons on each site. For simplicity we are assuming that the ions start in the entangled state and the noise is imposed at the two sites of entanglement. For  $N = 2$ , the Hilbert space consists of three states which are given by  $|0\rangle = |n_1 = 1, n_2 = 1\rangle$ ,

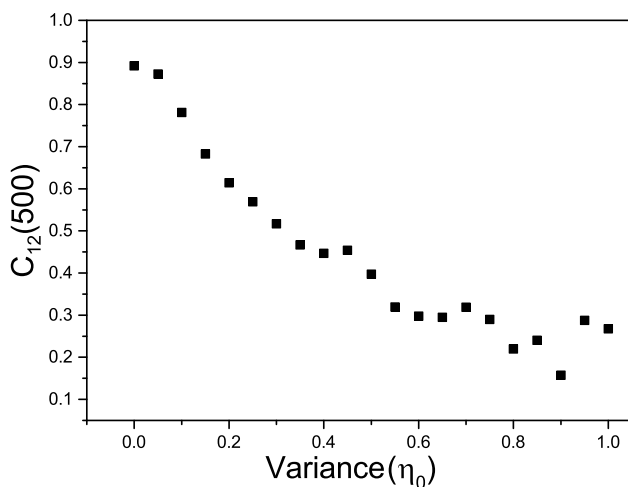


FIG. 11: (Color online) Plot of  $C_{14}(t_f = 500\hbar/|U^{(1)}|)$  with the effective noise temperature  $\eta_0$  in units of  $U_0$  showing the gradual decay of entanglement with larger noise temperature. The initial value of  $J/U_0$  is chosen to be 0.2 for this plot.

$|1\rangle \equiv |n_1 = 2, n_2 = 0\rangle$ , and  $|2\rangle = |n_1 = 0, n_2 = 2\rangle$ . Thus the state for the bosons at any time  $t$  during the dynamics and for a given realization of the noise  $\delta U$  can be written as

$$|\psi(t)\rangle = \sum_{\alpha=0}^2 c_\alpha(t)|\alpha\rangle \quad (24)$$

where the equations for the coefficients  $c_\alpha(t)$  can be obtained from the Schrodinger equation  $i\hbar\partial_t|\psi(t)\rangle = H_1(t)|\psi(t)\rangle$  and are given by

$$\begin{aligned} i\hbar\partial_t c_0 &= \sqrt{2}J(c_1 + c_2) \\ i\hbar\partial_t c_1 &= U(t)c_1 + \sqrt{2}Jc_0 \\ i\hbar\partial_t c_2 &= [U(t) + \delta U]c_2 + \sqrt{2}Jc_0. \end{aligned} \quad (25)$$

Eqs. 25 can be solved numerically to obtain  $c_\alpha(t)$  for a given disorder realization. The initial conditions for solving such equations can be obtained from finding their value for the system ground state at a fixed value of  $J/U^{(0)}$ . This can be done by numerical minimization of the system energy  $E = \langle\psi(0)|H(0)|\psi(0)\rangle$ .

Having obtained  $c_\alpha(t)$  for a given disorder realization, one can compute the cross correlation  $C_{12}^d$  given by

$$C_{12}^d(t) = \langle\psi(t)|(b_2^\dagger b_1)^2|\psi(t)\rangle/2 = c_1^* c_2 \quad (26)$$

One then averages  $C_{12}$  over several disorder realization and obtain  $C_{12}(t) = 2\text{Re}[\langle C_{12}^d(t) \rangle_d]$ , where the average is taken over  $M = 100$  realization of disorder. The behavior of  $C_{12}(t)$  as a function of the effective noise temperature  $\eta_0$  is shown in Fig. 11 for  $J_i/U^{(0)} = 0.2$  and  $t = 500\hbar/|U^{(1)}|$ . We note that the entanglement gradually decays from its value 0.9 for  $\eta_0 = 0$  to around 0.2 for  $\eta_0 = U^{(0)}$  with increasing  $\eta_0$ . In a typical experimental setup, the variation of the laser intensity and/or phase is around 1% and this leads to around 3% fluctuation in the value of  $U$ . This suggest that the experimental noise might lead to a reduction of  $\sim 10\%$  value of the cross correlation as obtained from the simple naive model. A more detailed analysis of this phenomenon which is expected to provide an accurate estimate of the entanglement reduction in a more realistic situation is left for future work.

In conclusion, we have studied the non-equilibrium dynamics of phonons in an ion trap and have shown that such dynamics, for carefully chosen protocol, may lead to both cooling and entanglement generation. We have provided a detailed analysis of theoretical method used to study such dynamics. Using this, we have identified the non-linear ramp protocol with exponent  $\alpha = 0.8$  to be optimal for both cooling and entanglement generation. Finally we have provided an estimate of cooling and entanglement generation times based on our analysis which may be confirmed in experiments and have also qualitatively discussed the effect of the presence of laser intensity fluctuations on the entanglement generation.

## VI. ACKNOWLEDGEMENT

MM and TD would like to acknowledge the financial support from National Research Foundation-Prime Min-

ister's Office, Singapore and the Ministry of Education, Singapore.

- 
- [1] E. E. Edwards *et al.*, Phys. Rev. B **82**, 060412(R) (2010); R. Islam *et al.*, Nat. Comm. **2**, 377 (2011).
- [2] D. Porras and J.I. Cirac, Phys. Rev. Lett. **93**, 263602 (2004).
- [3] S. Braun *et al.*, Science **339**, 52 (2013).
- [4] A. V. Steele, L. R. Churchill, P. F. Griffin and M. S. Chapman, Phys. Rev. A **75**, 053404 (2007).
- [5] X.-L. Deng, D. Porras, and J. I. Cirac, Phys. Rev. A **77**, 033403 (2008).
- [6] S. Sachdev, *Quantum Phase Transitions*, Cambridge University Press, Cambridge, England, (1999).
- [7] D. Porras and J.I. Cirac, Phys. Rev. Lett. **92**, 207901 (2004); G.-D. Lin, C. Monroe, and L.-M. Duan, Phys. Rev. Lett. **106**, 230402 (2011).
- [8] M. Greiner, O. Mandel, T. Esslinger, T. W. Hnsch1 and I. Bloch Nature **415**, 39 (2002); C. Orzel, A. K. Tuchman, M. L. Fenselau, M. Yasuda and M. A. Kasevich, Science **291**, 2386 (2001); T. Kinoshita, T. Wenger, and D. S. Weiss, Nature **440**, 900 (2006); L. E. Sadler, J. M. Higbie, S. R. Leslie, M. Vengalattore and D. M. Stamper-Kurn, Nature **443**, 312 (2006); W. S. Bakr *et al.*, Science **329**, 547 (2010); J. Simon *et al.*, Nature **472**, 307 (2011).
- [9] D. Jaksch, C. Bruder, J. I. Cirac, C. W. Gardiner, and P. Zoller, Phys. Rev. Lett. **81**, 3108 (1998).
- [10] S. Sachdev, K. Sengupta, and S.M. Girvin, Phys. Rev. B; M. Kobodurez, D. Pekker, B. K. Clark, and K. Sengupta, Phys. Rev. B **85**, 100505 (2012).
- [11] T. Dutta, M. Mukherjee, and K. Sengupta, Phys. Rev. A **85**, 063401 (2012).
- [12] T. Dutta, M. Mukherjee, and K. Sengupta, Phys. Rev. Lett. **111**, 170406 (2013).
- [13] D. De Munshi, T. Dutta, R. Rebhi and M. Mukherjee, Phys. Rev. A (R) *in print* (2015)
- [14] D. Leibfried, R. Blatt, C. Monroe, and D. Wineland, Rev. Mod. Phys. **75**, 281 (2003).
- [15] F. Dubin, D. Rotter, M. Mukherjee, C. Russo, J. Eschner, and R. Blatt, Phys. Rev. Lett. **98**, 183003 (2007).
- [16] D. F. A. James, Appl. Phys. B **66**, 181 (1998).
- [17] C. Kittel, *Quantum Theory of Solids*, Wiley and Sons, New York (1963).
- [18] See for example, A. del Campo and K. Sengupta, EPJST **224**, 189 (2015).